TAO, Supplementary Issue, 99-114, March 1999

The Atmospheric Effect Correction of the Ocean Color Imager of ROCSAT-1—Simulations and Using SeaWiFS Data as the Example

Gin-Rong Liu[1], Shih-Jen Huang[1], Tsung-Hua Kuo[1],
Wann-Jin Chen[2] and Chung-Yi Tseng[3]

(Manuscript received 10 December 1998, in final form 22 January 1999)

ABSTRACT

The total radiance observed by satellite-borne ocean color sensors results from several contributions: the atmospheric molecular and aerosol scattering, the sea surface reflectance and the water leaving radiance. In order to apply these ocean color sensor data to access the ocean parameters, atmospheric correction should be undertaken in advance to extract the water leaving radiance that is relevant to the ocean parameters. The aim of this study is to establish one atmospheric correction process for the Ocean Color Imager (OCI) of ROCSAT-1, and some pre-launch simulation results are demonstrated.

The simulation shows that the water leaving radiance estimation seems to be reliable by the ocean color radiance algorithm proposed in this paper, because the estimated total pigment concentration seems to be reasonable. Further investigations done in this study using SeaWiFS data reveal that the water leaving radiance is somewhat overestimated in comparison with ship measurements because of the underestimated aerosol scattering. The reason for this underestimation is probably the inconsistent marine aerosol type and size distribution between the real and input atmospheric parameters. The simulated result also shows the sun glint effect is significant and plays the most important role in the radiance contributions of OCI imagery. Consequently, choosing the most suitable acquiring time of OCI in order to avoid the sun glint effect will be very important in future OCI operation scheduling.

(Key words: OCI, Atmospheric correction, Water leaving radiance, Sun glint)

[1]Center for Space and Remote Sensing Research, National Central University, Chung-Li, Tao-Yuan, Taiwan, ROC

[2]Department of Applied Physics, Chung Cheng Institute of Technology, Ta-Shi, Tao-Yuan, Taiwan, ROC

[3]Institute of Physics, Academia Sinica, Taipei, Taiwan, ROC

1. INTRODUCTION

In the past several decades, applying satellite-borne visible and near-infrared sensors to determine ocean parameters, such as chlorophyll richness and ocean biomass, has been became one of the important applications in the remote sensing field. The Nimbus-7 Coastal Zone Color Scanner (CZCS) of the U.S.A. was the first sensor designed for ocean color monitoring. The analysis based on the total 66,000 CZCS images acquired by CZCS have provided much information concernig the relationships between radiance values and ocean chlorophyll amounts and other ocean parameters in the visible and near-infrared bands (Evan and Gordon, 1994). After this successful ocean color experiment, the second generation ocean color sensor, Sea-viewing Wide Field-of-view Sensor (SeaWiFS), mounted on SeaStar was launched in August 1997. SeaWiFS is one operational sensor and its propose is to collect global ocean color data for the estimation of chlorophyll content to understand the global variation (Gregg *et al*., 1993). Then, the Ocean Color and Temperature Scanner (OCTS) mounted on the MIDORI satellite of Japan was launched in 1996. Unfortunately, MIDORI lost contact with earth in June 1997. In the near future, the Moderate Resolution Imaging Spectrometer (MODIS) of the U.S.A. and the Ocean Color Imager (OCI) of the R.O.C. will be launched.

Generally OCI will be an ocean color sensor similar to SeaWiFS, and it will function as the first general science satellite in the ROCSAT series. OCI will use a six spectral band spanning all-refractive spectral-radiometer in visible and near infrared regions, and will be mounted on ROCSAT-1 and launched in the late January 1999. ROCSAT-1 will be a low-earth orbit science experimental satellite at the altitude of 600 km with an inclination of 35 degrees, and its period will be 97 minutes. OCI is a push-broom scanner with a field of view of about 700 km. Every OCI scan line consists of 896 sampling pixels. The ground resolution per pixel is about 800 meters and about 400 meters for the 64 nadir pixels. The six OCI channels' central wavelengths are 0.443, 0.490, 0.510, 0.555, 0.670, and 0.865 μm, respectively. Besides, one extra 0.555 channel is designed to monitor sensor decay. Because the OCI sensor consists of channels located in the visible and near-infrared regions, its channels will be influenced significantly by the effects of atmospheric aerosols and molecules, and reflected solar radiance. To apply the coming OCI data for ocean color and relevant applications accurately, an integrated, accurate atmospheric effect model should be developed to eliminate the probable atmospheric influences and obtain the accurate ocean parameter retrievals. The goal of this paper is to develop one such model. In section II, the theorems and algorithms involved in the atmospheric correction are discussed. In section III, the relative data and parameters are described. The results and analysis are reviewed in section IV, and the conclusions are made finally in section V.

2. THEOREM AND METHODOLOGY

In the visible and near-infrared regions, where the OCI channels are located, the atmospheric effects come mainly from atmospheric molecular Rayleigh scattering and atmospheric aerosol Mie scattering effects. Owing to the influence of these scattering effects, the total radiance observed by satellite-borne visible and infrared sensors is usually an ambiguous mixture of the atmospheric radiance and the target reflected radiance, which we are truly inter-

ested in. Therefore, how to reduce or eliminate the atmospheric radiance and extract the reflected target radiance from the satellite observing total radiance is the most essential task in OCI data applications.

According to the practical experiment and the analysis based upon the CZCS data, the total radiance, L_t, observed by satellite sensors is contributed by the Rayleigh scattering, L_r, the aerosol scattering, L_a, the atmospheric-influenced water leaving radiance, TL_w, and the sun glint effect, L_g, for some scanning period. Contrary to the CZCS sensor, the sun glint radiance will contribute more to the total radiance in some OCI scanning images, because the OCI sensor won't provide a way to avoid the sun glint effect. So, the radiance relation of satellite-borne sensor images in visible and infrared regions can be expressed as

$$L_t = L_r + L_a + L_g + TL_w \tag{1}$$

The analysis based upon CZCS data shows that generally the water leaving radiance is about 10 CZCS digital counts, the Rayleigh scattering is about 100 digital counts, the aerosol scattering contribution is about 10 digital counts in the thin optical depth atmospheric conditions, and can become very significant, up to 100 digital counts, in some thicker optical depth atmospheric conditions (Gordon and Wang, 1992). From the CZCS analysis, the various atmospheric effects can be indicated and their individual non-negligible contributions shown. Contrary to the obvious atmospheric radiance, the water leaving radiance frequently is a small portion of the total radiance. Consequently, an accurate atmospheric radiance computation procedure will be necessary to isolate the water leaving radiance from the total radiance in OCI channels for the future applications.

Based on the previous discussion, the OCI atmospheric effect computations can be partitioned and modeled into several parts, and then eliminated individually one by one. These parts include Rayleigh scattering, Mie scattering, sun glint effect, and water leaving radiance.

2.1 Rayleigh Scattering

Studies show that the approach of paralleled atmosphere used in the radiative transfer for the Rayleigh scattering computation would be not suitable when the solar zenith angle or satellite zenith angle is larger than 50 degrees, especially for the single scattering model (Gordon *et al*., 1988). Although the computation error would be reduced when the multi-scattering model is used, this alternative procedure seems to be impractical due to the extra computation time. Fortunately, the largest OCI scanning angle is 29.94° and its largest zenith angle is 32.08° . Meanwhile, the observing coverage of OCI is located between 38° N and 38° S. Thus, the solar zenith angle will be less than 50 degrees in most observing cases. So, the paralleled atmosphere approach and single scattering model will be reasonable for OCI-like sensors Rayleigh computation (Eckstein and Simpson, 1991), and can be written as

$$L_r(\lambda) = \frac{\tau'_{\mathrm{r}}(\lambda) F_0'(\lambda) P_a}{4\pi \cos\theta} \tag{2}$$

where $\tau_r'(\lambda)$ is the Rayleigh optical thickness in the different atmospheric pressures, P, and can be expressed as

$$\tau_r'(\lambda) = \tau_r(\lambda)\frac{P}{P_0} \tag{3}$$

where $\tau_r(\lambda)$ is the Rayleigh optical thickness in the standard atmospheric pressure P_0=1013.25 mb, and can be calculated again with

$$\tau_r(\lambda) = 0.008569\lambda^{-4}(1 + 0.0113\lambda^{-2} + 0.0013\lambda^{-4}) \tag{4}$$

where λ is wavelength in μm. $F_0'(\lambda)$ is the solar irradiance after extincting by atmosphere, P_a is the probability of the photos scattered by the atmosphere and transferred into the sensor, can be estimated by the following equation

$$P_a = P(\chi^-) + [\rho_n(\theta_0) + \rho_n(\theta)]P(\chi^+) \tag{5}$$

where $P(\chi^\pm)$ is the Rayleigh phase function, its function form is

$$P(\chi^\pm) = \frac{3}{4}(1 + Cos^2\chi^\pm) \tag{6}$$

where the $\chi^\pm$ is the scattering angle, it can be rewritten as

$$Cos\chi^\pm = \pm Cos\theta Cos\theta_0 - Sin\theta Sin\theta_0 Cos(\phi - \phi_0) \tag{7}$$

where θ and θ_0 are the zenith angles of sensor and solar at the measured point, respectively. ϕ and ϕ_0 are the azimuth angles of sensor and solar from the pixel. ρ_n is the Fresnel reflectivity of a flat sea surface

$$\rho_n(\eta) = 0.5\left[\frac{\sin^2(\eta - \eta_r)}{\sin^2(\eta + \eta_r)} + \frac{\tan^2(\eta - \eta_r)}{\tan^2(\eta + \eta_r)}\right] \tag{8}$$

where η_r is the reflectance angle, and can be calculated by using Snell's law. In this study, the sea water reflectivity is assumed to be n=1.341.

2.2 Aerosol Scattering

The single scattering radiance of atmospheric aerosol can be modeled as (Gordon and Castano, 1987)

$$L_a(\lambda) = \frac{\omega_a(\lambda)\tau_a(\lambda)F_0'(\lambda)P_a}{4\pi\cos\theta} \tag{9}$$

where $\omega_a(\lambda)$ is the single aerosol scattering albedo, and can be parameterized as (Gregg and Carder, 1990)

$$\omega_a(\lambda) = \omega_a(0.4)\exp\left[0.095[\ln(\lambda / 0.4)]^2\right] \tag{10}$$

$$\omega_a(0.55) = (-0.0032AM + 0.972)\exp(3.06 \times 10^{-4} RH) \tag{11}$$

where *AM* is the marine air mass characteristic parameter, and indicated from 1 to 10 for different air types. In general, larger *AM* values indicate the atmosphere is influenced more by the continental air mass. In the practical computations, *AM*=1 is indicates the open ocean and *AM*=10 indicates the atmosphere is influenced strongly by continental atmosphere. In the general case, the *AM* is set as 3 (Gathman, 1983), and *RH* is the atmospheric relative humidity.

In this study, the size distribution of marine contribution is modeled by using the following equation:

$$\sum_{i=1}^{3} A_i \exp\left[-\ln\left(\frac{r}{f\, r_{oi}}\right)\right]^2 / f = \frac{dN}{dr} = Cr^{\gamma} \tag{12}$$

where A_i is the amplitude function of size distribution, and is the function of aerosol type, air mass characteristic and sea surface wind speed. r_{o1}, r_{o2} and r_{o3} are the size radii of the size distribution center, and the values are 0.03 μm, 0.24 μm and 2.0 μm, respectively. *f* is the factor of size radii change versus the relative humidity.

Rewritten equation (12) becomes

$$\ln\left(\frac{dN}{dr}\right) = \ln C + \gamma \ln r \tag{13}$$

and let *r* be 0.1, 1.0 and 10.0 μm, respectively. The *dN*/*dr*, *C* and γ (Junge exponent) values then can derived by the Least Square method. In this paper, the Henyey-Greenstein phase function is used to compute the marine aerosol effect.

2.3 Air Mass Characteristic

For application of OCI data, this study paid attention to the atmospheric effect over ocean. Therefore, the special marine air mass characteristic will be one of important parameters in the modeling task. In practical cases, the marine air mass characteristic is difficult to measure routinely because it is expensive and requires much man-power. So, this study will try to develop a method to determine the air mass characteristic from the OCI image base. Basically the upwelling radiance from the sea surface of the near infrared channel can be assumed as almost zero. Based on this relation, Gordon and Clark (1981) assumed the water leaving radiance is zero over clean ocean in the CZCS 670nm near infrared channel, and derived the aerosol scattering effect. Because the OCI sensor has two near infrared channels, 670 and 865nm, the aerosol scattering effect also can be derived from these two channels. Basically the Rayleigh scattering can be calculated precisely by models. So, the air mass characteristic parameter can be determined by comparing the difference between the observed radiance and Rayleigh scattering radiance of 670 or 865nm channels

$$AM = 0.5109 + 30.0834(L_t - L_r) - 37.0919(L_t - L_r)^2 + 17.5908(L_t - L_r)^3 \tag{14}$$

Generally the *AM* value is determined by the L_t and L_r of the 865nm channel, but the 670nm

channel is used to replace the 865nm channel in some cases when the total radiance of the 865nm channel is zero.

2.4 Sun Glint Radiance

After Cox and Munk (1954a,b) used a statistical model to estimate the sea surface slope probability distribution, Viollier *et al*. (1980) assumed the sea surface aspect is near isotropic and displays Gaussion distribution, and showed the slope was only a function of sea surface wind speed. Using this approach, the sun glint effect can be estimated when the solar and sensor geometrical relation is known

$$L_g = \frac{\rho_t T_0(\lambda,\theta_0) T_0(\lambda,\theta) F_0(\lambda) P_w(\theta,\phi;\theta_0,\phi_0;W)}{4\cos\theta\cos^4\theta_n} \tag{15}$$

where $P_w(\theta,\phi;\theta_0,\phi_0;W)$ is the sun glint probability when sensor and solar are located at (θ,ϕ) and (θ_0,ϕ_0), respectively, W is the sea surface wind speed, ρ_t is the reflectivity of rough sea surface, $T_0(\lambda,\theta_0)$ and $T_0(\lambda,\theta)$ is the transmittance from solar to sea surface and from sea surface to sensor, respectively.

2.5 Water Leaving Radiance

When the Rayleigh, Mie and sun glint effect are estimated accurately, the water leaving radiance can be accessed. Because the real water leaving radiance observed by satellite sensor is influenced by the atmospheric effect, the real satellite observed total radiance observations have to be corrected by the atmospheric effect correction to get the normalized water leaving radiance (Gordon, 1993) , L_{wn} ,

$$L_{wn}(\lambda) = \frac{TL_w(\lambda)}{\cos\theta_0 \exp\left[-\left(\frac{\tau_r(\lambda)}{2}+\tau_{oz}(\lambda)\right)\left(\frac{1}{\cos\theta_0}+\frac{1}{\cos\theta}\right)\right]} \tag{16}$$

3. DATA AND SOURCE

For atmospheric effect modeling and preparing for the OCI image analysis, an atmospheric transmittance/radiance computation model, the Oceanic Color Imager Transmittance/radiance computation code (OCITRAN-2) was established in this study. This code was developed based on the OCITRAN-1 package developed by this team. This model is a mixing single/multi- scattering model. As mentioned in the previous discussion, single scattering computation is accurate enough for aerosol scattering computation. Therefore, OCITRAN-2 computes Rayleigh scattering in the single/multi-scattering mode, but computes aerosol scattering in the single scattering mode. This model calculates the aerosol scattering effect from the image-based concept discussed in section 2.3 that can reduce the required atmospheric parameter numbers.

Although some input parameters can be image-based, still some parameters are needed. This study uses some climate parameters provided by the Comprehensive Ocean-Atmosphere Data Set (CDADS), compiled by the National Oceanic and Atmospheric Administration (NOAA), the National Climatic Data Center (NCDC) and the National Center for Atmospheric Research (NCAR). Several parameters were input from the CDADS, such as air pressure, sea surface wind speed, precipitable water, relative humidity. These data were provided in 2.5 x 2.0 longitude x latitude grid form. Meanwhile, the ozone parameter was obtained from monthly mean Total Ozone Mapping Spectrometer data, and the resolution was 1.25 x 1.0 longitude x latitude grid.

Because the OCI sensor will launched in January 1999, to date no real OCI image is available. This study uses the SeaWiFS images to investigate the OCITRAN-2 accuracy. Of course, the OCITRAN-2 will be modified to suit SeaWiFS geometrical and radiative considerations. In order to investigate OCITRAN-2 accuracy, two SeaWiFS images, acquired at 04:27GMT, November 24, 1997 and 03:55GMT, January 13, 1998, were used in this test, and their ground resolution is 4.4km and 1.1km for the two SeaWiFS images, respectively. These two images both covered the Taiwan area.

Meanwhile, concurrent in-situ ship-measured water leaving radiance data were collected by the research vessel, Ocean Research II of the ROC National Science Council on November 24, 1997. The water leaving radiance related to the SeaWiFS channels was measured by the Satlanic TSRB-II and SPMR radiometers aboard on Ocean Research II.

4. RESULT AND ANALYSIS

Several steps were done with the SeaWiFS images in our procedure. Firstly, a cloud and land masking procedure was undertaken to screen the cloud and land pixels. Then, we calculated the sun glint probability and screened the pixels with a probability parameter larger than 1.5, indicating these pixels were influenced strongly by sun glint effect (McClain and Yeh, 1994). After screening the unsuitable pixels, we computed the Rayleigh scattering for SeaWiFS channels. Then, we determined the air mass characteristic parameter with the 670 and 865nm channels. Then, the aerosol scattering effect was calculated and the water leaving radiance was estimated finally.

Table 1 shows the comparison of water leaving radiance estimated by OCITRAN-2 and

Table 1. The comparison of ship-measured, SeaDAS-estimated and OCITRAN-estimated water leaving radiance. Ship-measuring time was 0427GMT, November 24, 1997, and sampling location was (25.46N, 122.27E). Unit in $mW/cm^2/\mu m/sr$.

SeaWiFS Channel	ship-measured	SeaDAS	OCITRAN2
443 nm	1.435	0.669	2.1
490 nm	1.408	0.657	1.8
510 nm	1.084	0.640	1.5
555 nm	0.574	0.571	0.7

the SeaDAS model, and ship-measured radiance in four SeaWiFS channels. The SeaDAS model is an official model developed by SeaWiFS project for the SeaWiFS atmospheric effect correcting. The comparison shows that OCITRAN-2 derived water leaving radiance is over-estimated somewhat by 46%, 28%, 38% and 22% in the tested four channels, and SeaDAS derived radiance in 555nm channel is close to the ship-measured but that in other channels is under-estimated by 53%, 53%, and 41%. The result reveals that the OCITRAN-2 has reasonable accuracy when comparing the field measured data to the SeaDAS model estimation.

For the other SeaWiFS images acquired on January 13, 1998, the ship-measured experiment failed because the sample location was cloudy. This study only used this image as the input of the OCITRAN-2 model. Overall the retrieved water leaving radiance and total pigment concentration estimates seemed to be reasonable, but more precise comparison couldn't be made because of lost ship-measured data.

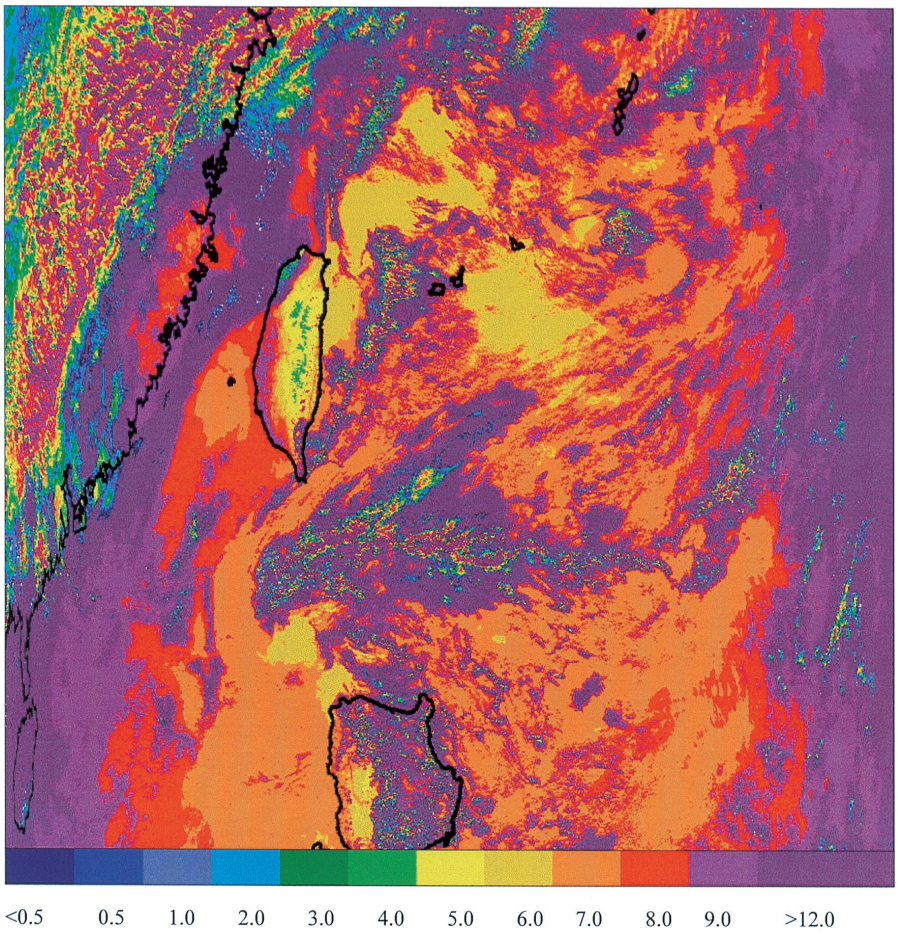

Fig. 1. The total radiance of SeaWiFS 443nm channel image of January 13, 1998. Unit in $mW/cm^2/\mu m/sr$.

After verifying the OCITRAN-2 accuracy, this study used the OCITRAN-2 and SeaWiFS images to retrieve the water leaving radiance. Figure 1 and 2 are the total radiance map and the estimated normalized water leaving radiance map, respectively. In this step, the 865nm channel image was used to screen the cloud pixels. The white pixel part in Figure 2 indicates the cloudy area. The map shows that the water leaving radiance map has higher values around the Taiwan Strait area and about 2-3 $mW/cm^2\,\mu msr$,and is about 1-2 $mW/cm^2\,\mu msr$ around other areas. The estimated total pigment concentration map also shows higher values around the Taiwan Strait area (not shown), especially around the northern ocean area of Peng-Hu. The higher values pixels were probably caused by higher suspended solid (S.S.) concentration around these areas.

Based on several studies and this OCITRAN-2 simulation, it's clear that the sun glint effect plays a very important role in the water leaving radiance retrieval because the OCI

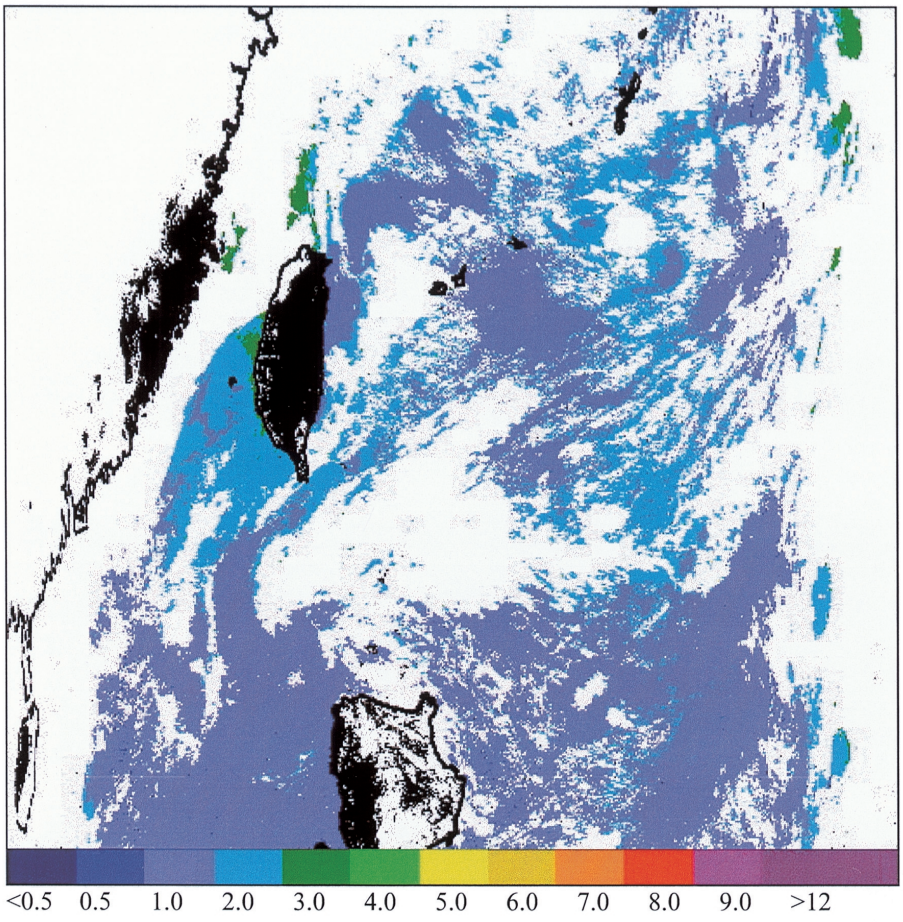

Fig. 2. Same as Figure 1, except for the OCITRAN-2-estimated water leaving radiance in 443nm.

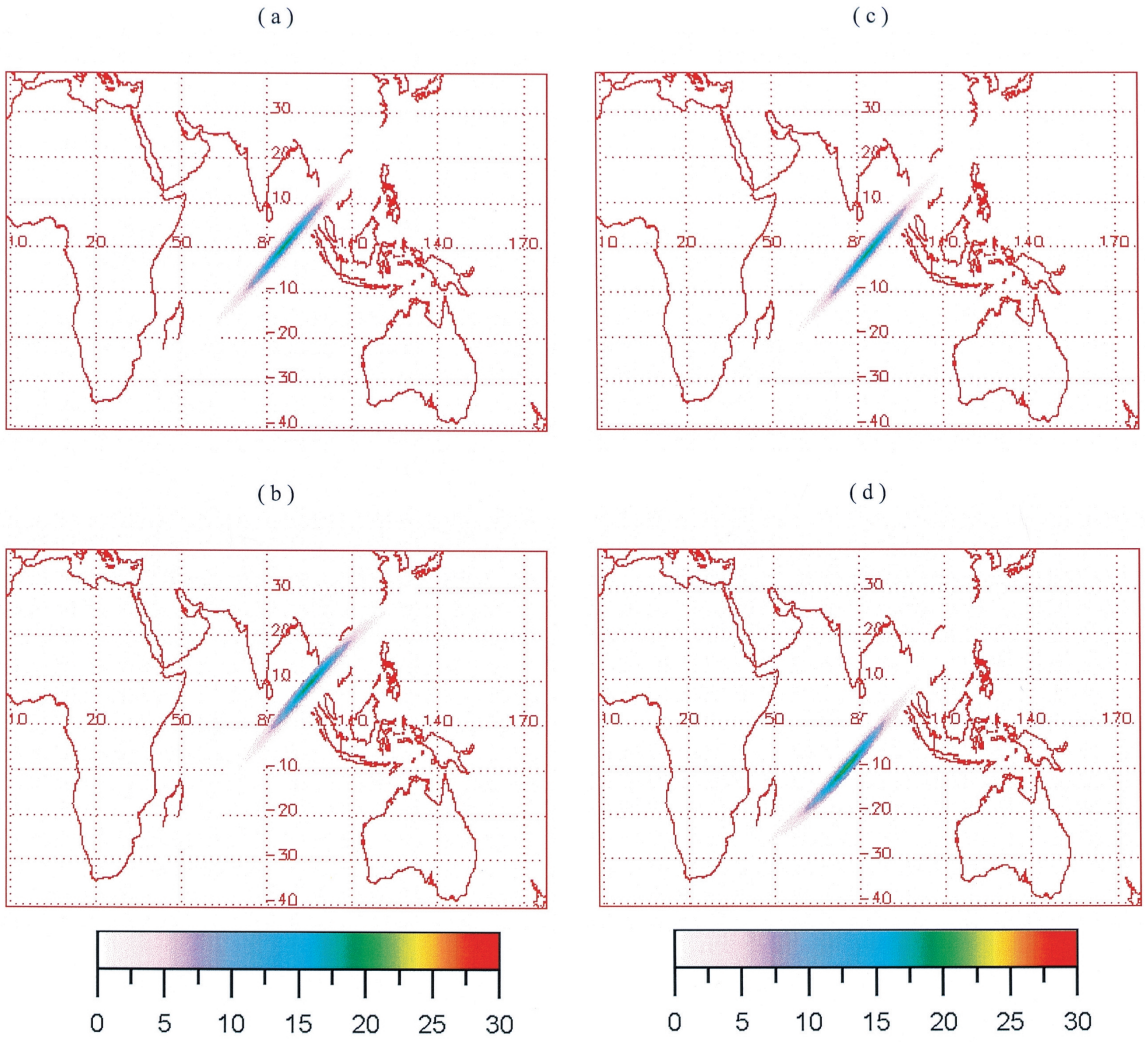

Fig. 3. The simulated sun glint radiance images of OCI 443nm channels. The equatorial ascending time is 12:00 and sea surface wind speed is 3m/sec, (a)Spring Equinox, (b) Summer Solstice, (c) Autumn Equinox, (d) Winter Solstice.

sensor can't provide a way to avoid the sun glint effect. To investigate the sun glint effect in OCI images, this study used the OCITRAN-2 model to simulate the sun glint effect observed from OCI sensor. The testing days fell on the Spring Equinox, Summer Solstice, Autumn Equinox and Winter Solstice, respectively, and the Cross Equatorial Time (CET) was local time 12:00 in the Ascending mode. The OCI scanning time was local time from 9:00 to 15:00. The sea surface wind speed was 3 m/sec. The four simulated sun glint radiance maps and water leaving radiance are shown in Figure 3 and 4. On the Spring Equinox and Autumn

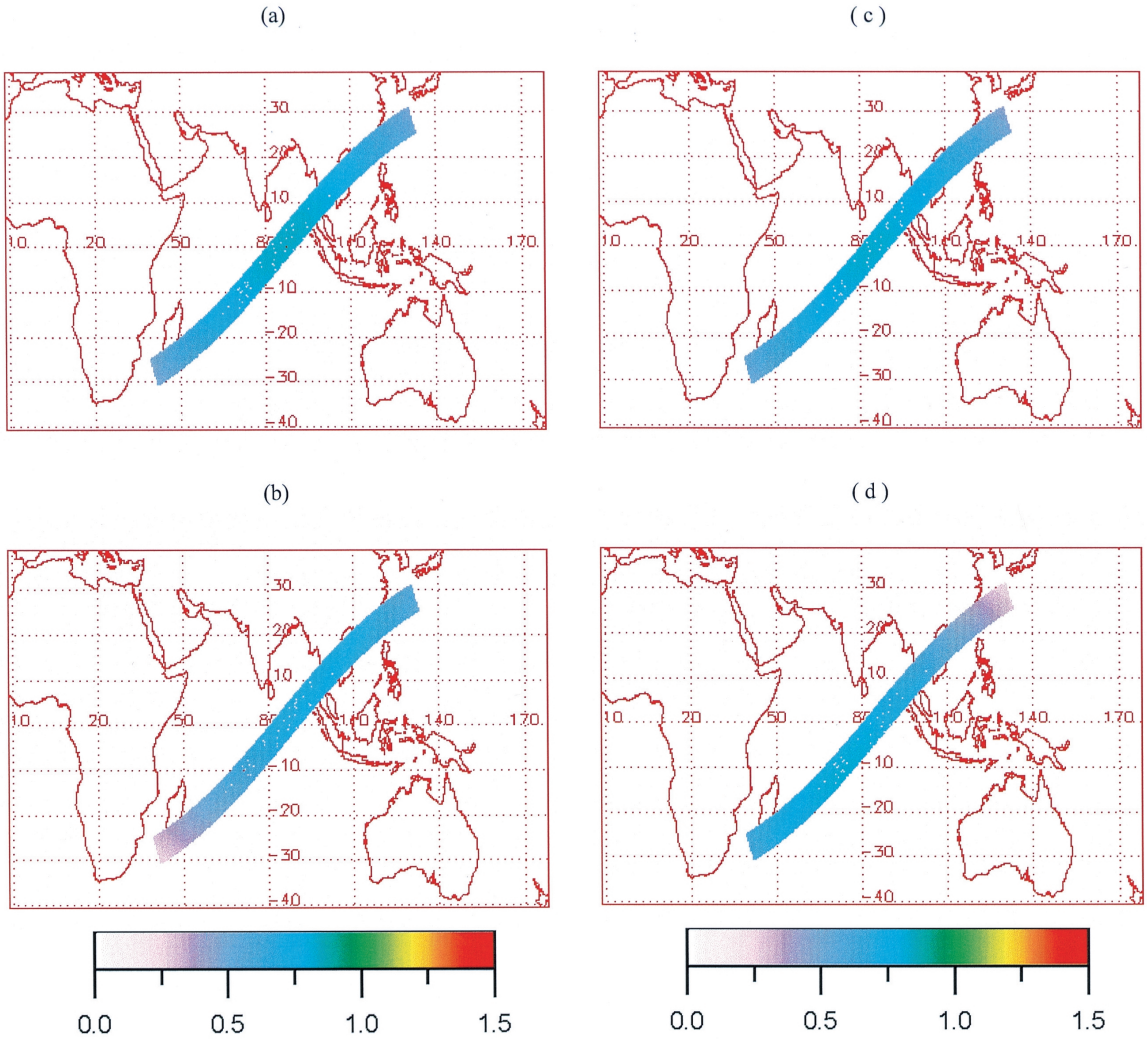

Fig. 4. Same as Figure 3, except for the water leaving radiance.

Equinox days, the maps show that the sun glint effects are very significant between 15° S to 15° N (Figure 3(a) and 3(c)), and the water leaving radiance is higher around the equator areas (Figure 4(a) and 4(c)). The sun glint effect appears maximum around the area between 6° S to 22° N on the Summer Solstice period (Figure 3(b)), and the water leaving radiance has larger radiance around the solar location area (Figure 4(b)). In the Winter Solstice period, the sun glint area and maximal water leaving radiance area moves to areas 22° S to 6° S (Figure 3(d) and 4(d)). To understand the contribution of sun glint effect, the comparison of sun glint effect to the total radiance of the simulated OCI images are shown (Figure 5). The left panels of Figure 5 are the radiance change in along-track pixels, and the right panels are the radiance change in cross-track pixels.

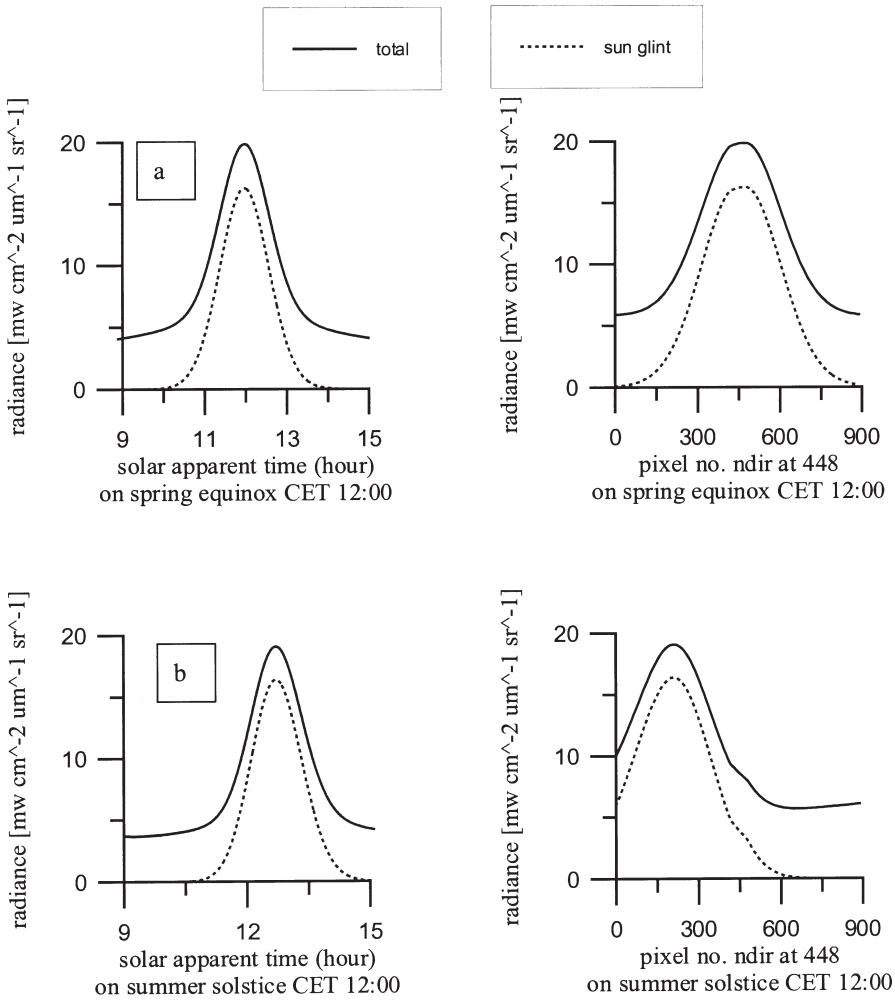

Fig. 5. The comparison of OCI 443nm channel total radiance and sun glint radiance. The simulated conditions were same as Figure 3.

This study also tested the sun glint effect and water leaving radiance change during different CET conditions. The CET were local time 9:00 and 15:00 in Summer Solstice (see Figure 5 and 6). The result shows the sun glint area and water leaving radiance location; values vary obviously for the different CET. This means suitable OCI scanning times can be set in advance by model simulation to avoid the sun glint effect.

5. CONCLUSIONS

Generally the results simulated by using the OCITRAN-2 model are reasonable and practical. The simulation and analysis show that the single Rayleigh scattering model can be used in

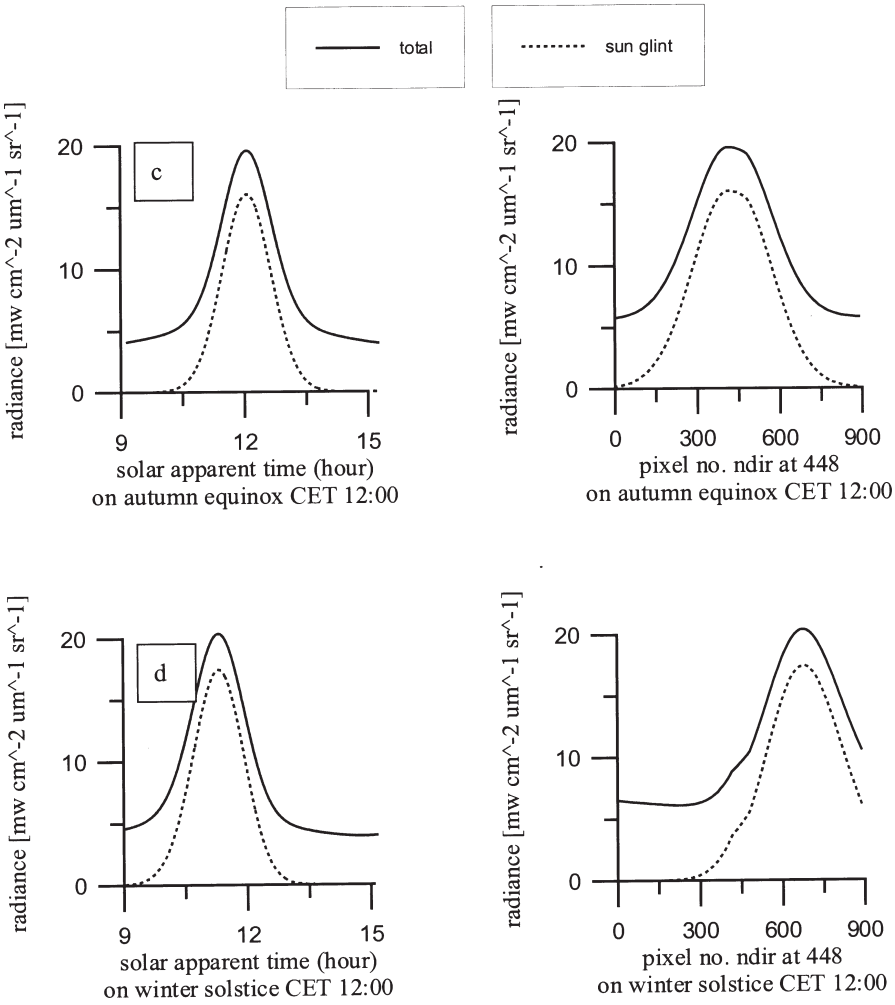

Fig. 5. (Continued)

OCI channel atmospheric correction to reduce the computation time. Of course, some further improvements in aerosol effect estimation are needed. The comparison between OCITRAN-2 simulations and SeaDAS model and field measurements show that the water leaving radiance result is rather reliable. Meanwhile, total pigment concentration accessed by this study is also quite reasonable, except for some overestimation in water leaving radiance, probably due to the inconsistent marine air mass characteristic. Because some input parameters were input with the climate database, some errors were probably induced. So, more field measurements are needed to check simulation results. Moreover, another task for the future will be how to reduce computation time and improve computation accuracy in this OCITRAN-2 module.

Because OCI sensor does not provide a way to avoid sun glint area, the simulation done by this study reveals that the effect of sun glint is significant and can not be neglected. In fact,

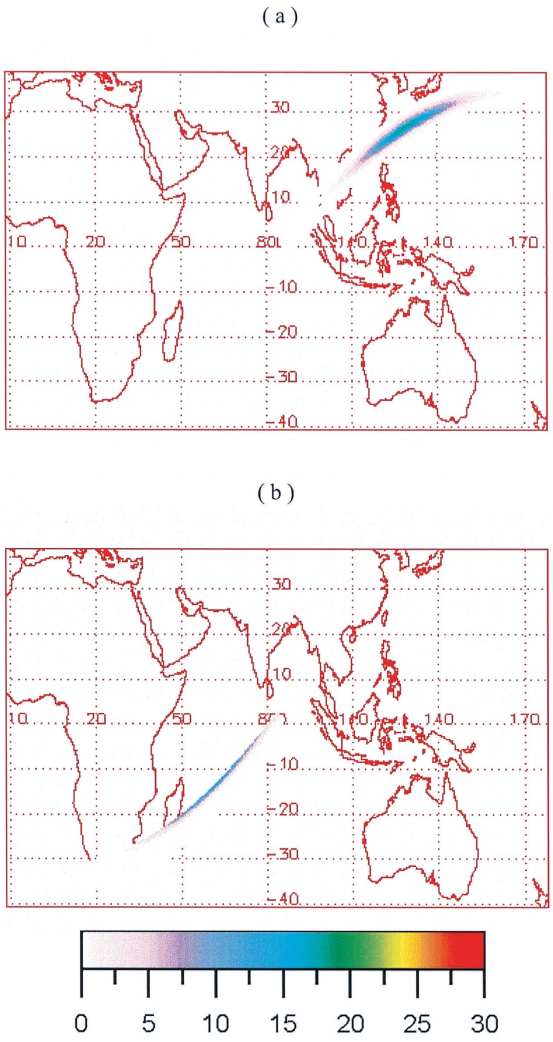

Fig. 6. Same as Figure 3, but (a) for Summer Solstice in 9:00 CET, (b) for Summer Solstice in 15:00 CET.

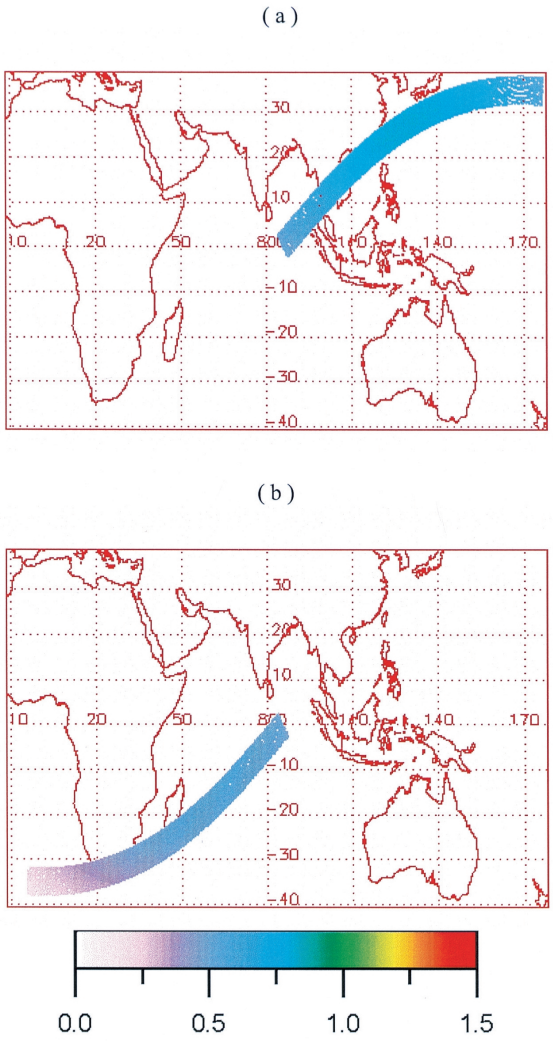

Fig. 7. Same as Figure 6, but for water leaving radiance.

the sun glint effect makes the most important contribution to the total radiance at some scanning times. Therefore, setting a proper OCI scanning schedule can improve OCI data quality significantly.

Acknowledgments The authors would like to thank Dr. C. R. McClain of the Goddard Distributed Active Archive Center (DAAC) funded through the NASA Earth Observing System (EOS) for providing the SeaWiFS image data, and Dr. Hsien-Wen Li of National Taiwan

Ocean University for assistance in obtaining field measured radiometric data with the research vessel Ocean Researcher II. Of course, many thanks are due to the crew and marine technicians aboard the research ship. This study was made possible by support from the National

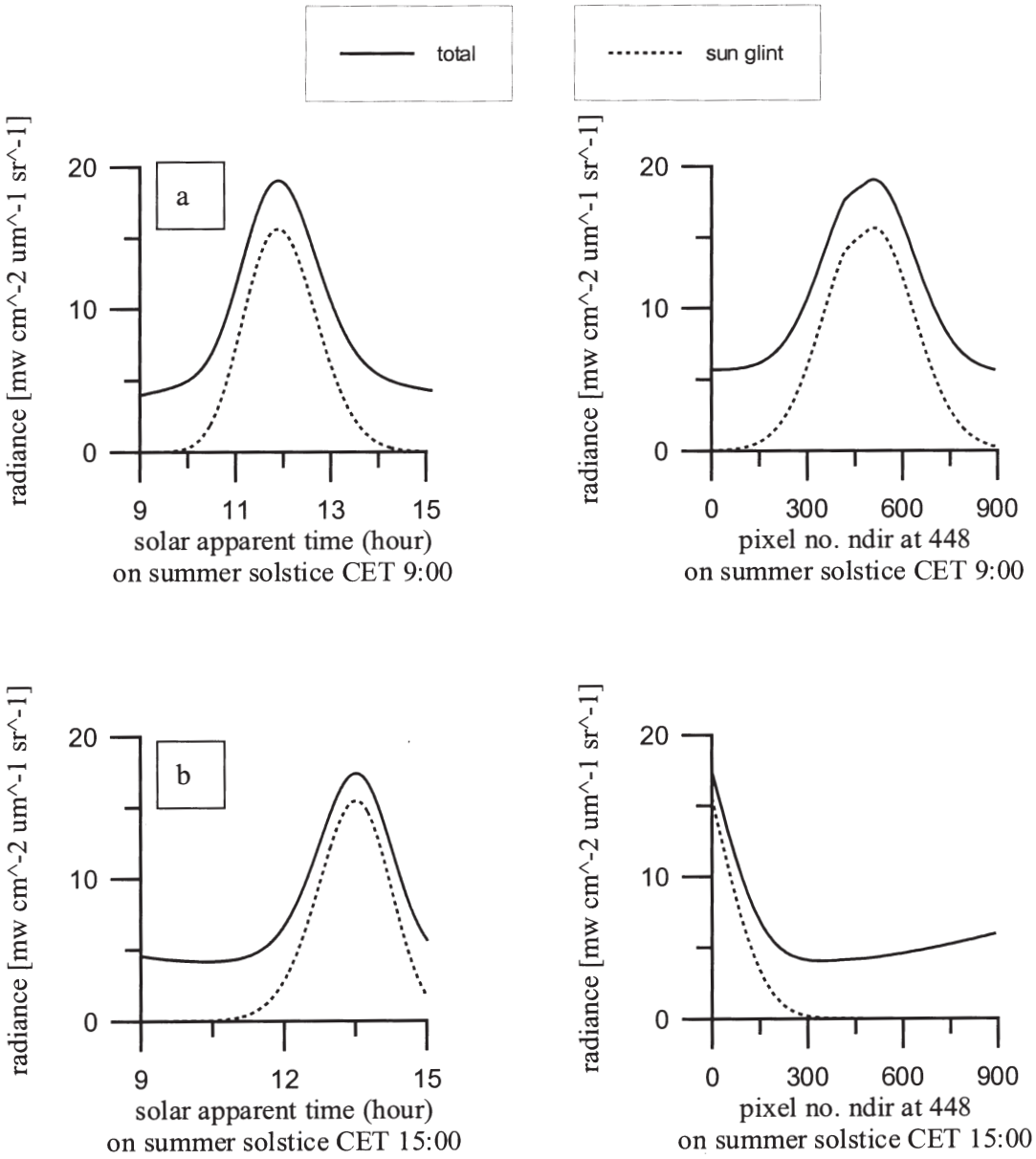

Fig. 8. The comparison of OCI 443nm channel total radiance and sun glint radiance. (a) Summer Solstice in 9:00 CET, (b) Summer Solstice in 15:00 CET.

Space Program Office (NSPO) of the National Science Council of Taiwan, R.O.C., which grant No. is NSC-86-NSPO-A-OCI-019-01-01 .

REFERENCES

Cox, C. and W. Munk, 1954a: Measurement of the roughness of the sea surface from photographs of the sun's glitter. *J. Opt. Soc. Am.,* **44**, 838-850.

Cox, C. and W. Munk, 1954b: Statistics of the sea surface derived from sun glitter. *J. Mar. Res.,* **13**,198-277.

Eckstein, B. A. and J. J. Simpson, 1991: Aerosol and Rayleigh radiance contributions to coastal zone color scanner images. *Int. J. Remote Sensing,* **12**, 135-168.

Evans, R. H. and H. R. Gordon, 1994: Coastal zone color scanner "system calibration": A retrospective examination. *J. Geophys. Res.,* **99**, 7293-7307.

Gathman, S. G. 1983: Optical properties of the marine aerosol as predicted by the Navy model. *Optical Engineering,* **22**, 57-62.

Gordon, H. R., 1993: Radiative transfer in the atmosphere for correction of ocean color remote sensors. In: Barale and Schilittenhardt (Eds.), Ocean Colour, 33-78.

Gordon, H. E. and D. K. Clark, 1981: Clear water radiances for atmospheric correction of coastal zone color scanner imagery. *Appl. Opt.,* **20**, 4175-4180.

Gordon, H. R. and D. J. Castano, 1987: Coastal zone color scanner atmospheric correction algorithm: multiple scattering effects. *Appl. Opt.,* **26**, 2111-2122.

Gordon, H. R., J. W. Brown and O. B. Evans, 1988: Exact Rayleigh scattering calculations for use with the Nimbus-7 coastal zone color scanner. *Appl. Opt.,* **27**, 862-871.

Gordon H. R. and M. Wang , 1992 : Surface-roughness considerations for atmospheric correction of ocean color sensors. I: The Rayleighscattering component. *Appl. Opt.,* **31**, 4247-4260.

Gregg, W. W. and K. L. Carder,1990: A simple spectral solar irradiance model for cloudless maritime atmospheres. *Limnol. Oceanogr.,* **35**, 1657-1675.

Gregg, W. W., F. C. Chen, A. L. Mezaache, J. D. Chen and J. A. Whiting, 1993:The simulated SeaWiFS data set, version1, SeaWiFS Technical Report Series, Vol 9.

Kneizys, F. X., E. P. Shettle, L.W. Abreu, G. P. Anderson, J. H. Chetwynd, W.O. Gallery, J.E.A. Selby and S.A. Clough, 1988: User Guide to LOWTRAN 7 , AFGL-TR 880177 Environmental Research Papers, No. 1010.

McClain, C. R. and E. N. Yeh, 1994: Sun Glint Flag Sensitivity Study, SeaWiFS Technical Report Series, Vol 13.

Viollier, M., D. Tanre and P. Y. Deschamps, 1980: An algorithm for remote sensing of water color from space. *Boundary-Layer Meteorology,* **18**, 247-267.